IET Energy Systems Integration

*Research Article*

IET Journals
The Institution of Engineering and Technology

# Innovative primary frequency control in low-inertia power systems based on wide-area RoCoF sharing

eISSN 2516-8401
Received on 2nd January 2020
Accepted on 12th February 2020
E-First on 12th March 2020
doi: 10.1049/iet-esi.2020.0001
www.ietdl.org

*Harold R. Chamorro[1] ✉, Felix Rafael Segundo Sevilla[2], Francisco Gonzalez-Longatt[3], Kumars Rouzbehi[4], Hector Chavez[5], Vijay K. Sood[6]*

[1]*KTH, Royal Institute of Technology, Stockholm, Sweden*
[2]*Power Systems and Smart Grid Lab at the Zurich University of Applied Sciences, Zurich, Switzerland*
[3]*University of South-Eastern Norway, Porsgrunn, Norway*
[4]*Seville University, Seville, Spain*
[5]*Department of Electrical Engineering, University of Santiago, Santiago, Chile*
[6]*Department of Electrical and Computer Engineering, University of Ontario, Institute of Technology, Ontario, Canada*
✉ *E-mail: hr.chamo@ieee.org*

**Abstract:** Future plans for integration of large non-synchronous generation and the expansion of the power system in the Nordic countries are a concern to transmission system operators due to the common interconnections and electricity exchanges among these operative areas. The expected reduction in the inertia anticipates an alteration of the frequency response, provoking a high Rate of Change of Frequency (RoCoF) slopes that can jeopardise the security of the interconnected systems. Since power generation in the Nordic countries such as Sweden, Finland and Norway is hydro-dominated, here, the authors propose a novel solution to tackle this problem including wide area measurements to monitor and share the RoCoF in remote areas with lower inertia to enhance their primary frequency control. To demonstrate the effectiveness of the proposed solution, first a test benchmark control with optimised parameters is developed and later compared against the proposed method. Additionally, since the proposed solution is based on measurements from remote locations in order to guarantee the stability of the system the impact of delays in the communication channels is also included in the problem formulation.

## 1 Introduction

The global electrical system is on the cusp of transition due to the current increase in renewable interconnection to the grid [1]. This transition is driven primarily due to the technological development of high-voltage direct current and sophisticated wide area measurement systems (WAMS) [2, 3]. However, the implementation of such technological advances is not straightforward due to different operational challenges related to WAMS, which is discussed and faced in this brief. One of the main issues expected from the massive penetration of renewable energy sources is the inertia reduction [4], which might result in larger frequency deviations from the nominal system frequency under a disturbance [5]. Maintaining the frequency stability within appropriate boundaries and providing an adequate response are of major importance, since reaching the system boundaries may provoke supply interruptions, which can eventually turn on lack of electricity, also known as blackouts [6]. Traditionally, hydro-power plants are the first option to contribute the most on frequency control in power systems due to its capability to quickly control the water flowing in the turbines through its governor. Hydro-controls, also known as hydro-governors, are modelled using transfer functions of first order composed by gains and time constants [7]. In order to address this challenge and improve the hydro-governor's actions, two groups of techniques have been observed in the literature. The first group corresponds to the use of optimisation methods and the second to the controller's realisation. There are benefits and drawbacks in both directions, which are briefly described next.

Evolutionary algorithms such as genetic algorithms have been applied in [8], in which the droop governor controller has been optimised. The secondary frequency response error was specially improved; however, the overshoot, settling time and oscillation damping were not included in the optimisation functions. Abdolmaleki *et al*. [9] tuned the droop gain using pole placement for load frequency control in hydro-power plants. However, even though this shows an improvement in the frequency response, the optimisation function was absent. A fractional order proportional integral derivative (PID) controller, optimised using the social spider optimisation algorithm, for secondary control in power systems incorporating distributed generation, is presented in [10]. In this case, the optimisation function involved frequency deviation in the connected areas and the results demonstrated an improvement in the frequency response, including a wind power model. However, the inertia was not analysed. A swarm-based algorithm, applied to the governor tuning parameters for frequency regulation, is proposed in [11]. The computing simulation results were performed for an actual hydro-power plant installation.

On the other hand, regarding the realisation controller's approach, the authors in [12] proposed a robust control based on a high-gain observer as an adjustable parameter to obtain an adequate dynamic response from a disturbance. A decentralised control signal for hydro-governors has been designed using $H_\infty$ control in [13], showing the speed response during different disturbances. By using a feedback linear approach, the authors in [14] aimed to design a governor to deal with the transient stability and to damp the oscillations in the system used. The authors in [15] presented a robust control design for hydro-governors based on additional inner states' feedback signals and this is compared with traditional PI and PID architectures. In [16], a fuzzy PID control structure is designed showing the possibility of including the derivative term as an extra signal involved in the hydro-governor control.

These above-mentioned contributions show that optimal governor controllers can be a general improvement to the primary frequency control; however, this is a provisional solution, especially when the non-synchronous generation is increasing continuously and the grid dynamics are changing. Therefore, the motivation of this research presents an innovative solution using Rate of Change of Frequency (RoCoF) measurements. Traditionally, maximum RoCoF is used to trigger local protection


This is an open access article published by the IET and Tianjin University under the Creative Commons Attribution-NonCommercial-NoDerivs License
(http://creativecommons.org/licenses/by-nc-nd/3.0/)

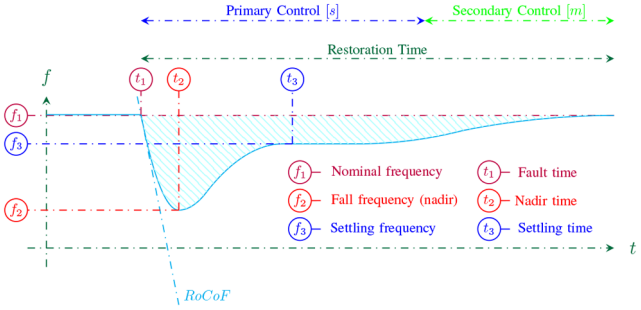


**Fig. 1** *Power system frequency response*

schemes; however in this work, we make use of the so-called average RoCoF calculated for one area and then compared with different areas in order to provide actions for triggering a centralised control scheme. Moreover, a power system/power plant with larger system inertia will be more resilient to frequency disturbances than a power system with smaller system inertia. However, if the RoCoF following a frequency deviation has a steeper slope, this measurement can be taken as an advantage to improve the controller's reaction in another/different interconnected region through WAMS, improving the general frequency response in the entire system. The evidence of different RoCoF slopes has been found in the national grid system in the UK and the Eirgrid in Ireland, where geographically separated frequency measurements exhibit such behaviour [17, 18]. Such geographic sparseness of inertia can provoke further larger frequency excursions and separation stability risks [19].

Another example of inertial frequency different responses in neighbours tie-line communicated countries is seen in the Central American region, where power outages in any of the neighbouring countries cause strong frequency imbalances [20]. This geographical–electrical mismatch can actually provide an innovative solution for low-inertia interconnected systems, the wide-area RoCoF sharing (WARS). Since the inertia of a power system/power plant affects the RoCoF following a system event, another possible improvement to counteract the large penetration of non-synchronous generation is by adding remote/supplementary RoCoF measurements with stepper slopes to the local ones, thereby altering the controller's reaction according to the low-inertia geographical zones that are interconnected. The relationship between system inertia and RoCoF can be illustrated through the swing equation shown in

$$2H \times \text{RoCoF} = \Delta P \tag{1}$$

where $H$ is the total inertia constant of the system (one or several interconnected) and $\Delta P$ is the total power change.

To give further context to the work in this paper, since fast-responding hydro-power plants have been used to efficiently and reliably add non-synchronous generation to electric power systems, many of the governors in use in Sweden are being upgrading processes from mechanical to automated controllers [21, 22].

Motivated by this challenge, and the increase in non-synchronous installations, which reduces the inertia in the system, this paper proposes a novel approach to counteract such dynamic changes. A WAMS to share the RoCoF signal (WARS) from areas with steeper slopes to other areas, in order to invoke a faster reaction in remote hydro-governors, which altogether contribute to the frequency response in the centre of inertia (CoI) frame. This WARS method is then compared with another method with the optimal hydro-governor parameters being obtained by a simulated annealing algorithm (SAA) optimisation method. Two different comparative signals are proposed: (i) the RoCoF average value obtained from local and remote measurements and (ii) the maximum absolute value of the local and remote RoCoF measurements. Moreover, the sub-systems stability and the impact of the delay in the communication channel are analysed. The proposed methods are tested and compared in a benchmark system that emulates the Nordic system frequency response.

A preliminary version of this work has been published in [23], where a networked control system has been proposed to counteract the non-synchronous generation integration. This work contains substantial differences to the proposed method and new simulations that do not appear in [23]. In contrast to [23], this paper focuses on using WAMS to share the inertia from low-inertia areas in order to improve the overall primary frequency control. Moreover, the theoretical frame and optimisation characteristics are also given.

The paper is organised as follows: in Section 2, the frequency response, the performance metrics and the measurement metrics are introduced. Section 4 presents the proposed method for reinforcing the primary frequency control to counteract the potential inertia reduction. Section 3 presents the perspective of low-inertia power systems modelling and establishes the test benchmark system. Section 6 presents the simulation results considering an aggregated model of the Nordic system, where three different operational areas are interconnected. In one of the areas, the inertia has been reduced in order to apply the RoCoF sharing method and, observe the impact on the system frequency control, and the improvement by the presented method is shown. Finally, the conclusions and future work are given.

## 2 Power system preliminaries

### *2.1 Power system frequency response*

In the joint Nordic system (Finland, Sweden, Norway and East Denmark), the obligations for maintaining reserves have been agreed in the System Operation Agreement between the Nordic transmission system operators (TSOs).

Electricity production must be equal to electricity consumption at all times. The balance between production and consumption is indicated by the frequency of the electricity grid which has a nominal value of 50.0 Hz. The market operators plan and balance their consumption and production in advance, but in practice there are deviations during each hour [24].

In a synchronous system, in the case of losing a generating unit, the frequency drops because of the imbalance between generation and load. Fig. 1 shows the dynamic response of the system frequency after disconnection of one generator for a typical system. The dynamic response is divided into two periods: Primary and secondary control response periods. During the first period, the inertial response of the spinning machines in the entire system reacts releasing or storing of kinetic energy tend to reduce the frequency deviation. System inertia is defined as the total amount of kinetic energy stored in all the rotating masses.

The inertial constant of an individual generator can be interpreted as the time that generator can provide full output power from its stored kinetic energy, taking values between 2 and 9 s typically.

Beyond the inertial response, the frequency is stabilised and then restored to the nominal frequency by the frequency containment reserve (FCR) by governor action and secondary controllers, respectively. The FCR acts as a proportional controller avoiding large frequency deviations; however, due to its control characteristic, it retains a steady-state error. The time response of this control is given in seconds (typically <30 s).

The aim of FCR is to stabilise frequency disturbances in the entire (internationally) connected high-voltage grid, regardless of the cause and location of disruptions. Severe frequency disturbances can lead to automatic load shedding and in the worst case cause a blackout. FCR is used for the constant control of frequency and it can be classified into two categories: FCR for normal operation (FCR-N) and FCR for disturbance (FCR-D) [25]. The FCR-N and FCR-D are momentarily available active power for frequency regulations and are activated automatically by the system frequency. However, FCR-D reacts under a long disturbance and it is associated with the governors action. FCR-N and FCR-D both have their own market. Note that the one developed in this document is in the frame of FCR-D [26].

Frequency restoration reserves returns the frequency back to its nominal value and also restores the reserves; its deployed time frame is given in minutes.


This is an open access article published by the IET and Tianjin University under the Creative Commons Attribution-NonCommercial-NoDerivs License
(http://creativecommons.org/licenses/by-nc-nd/3.0/)

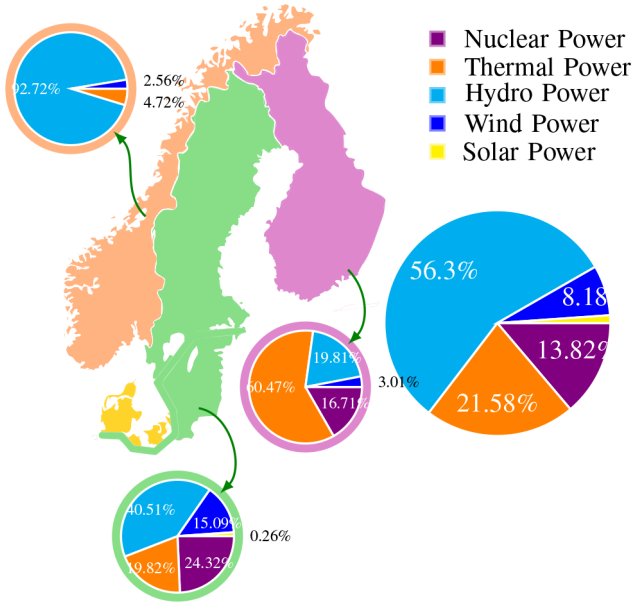


**Fig. 2** *Nordic countries power generation*

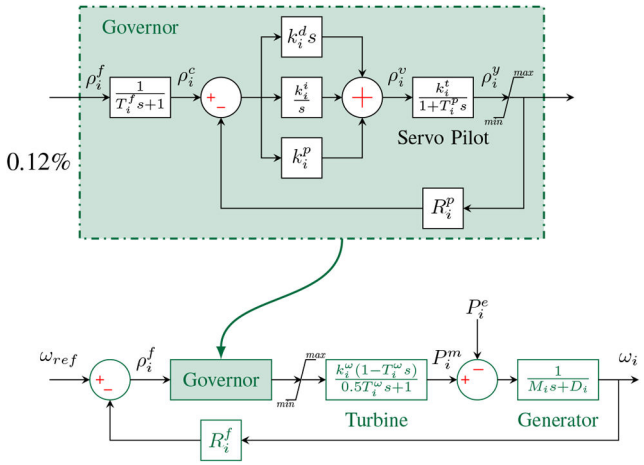


**Fig. 3** *System model*

### 2.2 Performance metrics

Following a disturbance in the system, in particular given a negative step disturbance such as a sudden load increase or generation drop at $t = t_1$, the following metrics are defined for quantifying the action of the distributed control action:

- *Nadir* is the maximum dynamic frequency deviation following an active power disturbance/contingency. It is dominated by the system inertia and governors response. Employing the optimal governor parameters, the frequency nadir can be reduced.
- Nadir time is the associated time $t = t_2$ to the nadir occurrence.
- Settling time $t = t_3$ is used to study the transient condition and to having a time mark to evaluate the control action on the settling frequency.

The objective is to reduce the nadir and decrease the time difference between $t_2$ and $t_3$ to an appropriate margin where it is improving the response reaction and to avoid any oscillations in the response.

### 2.3 Measurement metrics

In order to have an aggregated measurement of the frequency of an entire interconnected system, the CoI is used, which is computed based on the individual speeds $\omega_i$ and the inertia constants of the synchronous generators $H_i$.

Assuming the set $\mathcal{G}$ of synchronous generators, the expression to compute the CoI is

$$\omega_{\text{CoI}} = \frac{\Sigma_{i \in \mathcal{G}} H_i \omega_i}{\Sigma_{i \in \mathcal{G}} H_i} \tag{2}$$

In a similar manner, the RoCoF measurement in the CoI reference is defined as

$$\frac{\mathrm{d}\omega_{\text{CoI}}}{\mathrm{d}t} = \frac{\Sigma_{i \in \mathcal{G}} H_i (\mathrm{d}\omega_i / \mathrm{d}t)}{\Sigma_{i \in \mathcal{G}} H_i} \tag{3}$$

In addition, since (2) and (3) cover only a power system sub-network (e.g. country or region), then several CoI-referred RoCoF measurements should be gathered and shared from the sub-networks involved. For instance, a power system network with two established operative areas has two $\text{RoCoF}_{\text{CoI}}$ measurements to be used. However, it is worth mentioning that the values that sub-CoI-referred RoCoF system might reach depend on the system dynamic configuration, the contingency magnitude and location, the fault clearing time and the power system controllers installed in the system.

## 3 Low-inertia power system modelling

### 3.1 Non-synchronous generation integration

The Nordic power system (NPS) bases its power production on several renewable generation sources [27]. Base power demand in Sweden and Finland is, to a great extent, provided by nuclear production; while Norway's main source is hydro-production [28]. Considering the installed capacity of the three countries in the NPS, the different sources of electricity are shown in Fig. 2. The contribution by various generation sources of power per country is provided in their respective pie charts, as well as the aggregated sum.

As the European region seeks to increase its non-synchronous generation, several countries will inject more wind power in the future, thus reducing the operational frequency response capacity under possible imbalances [29]. Considering future reductions or even total shut down of the nuclear thermal units being replaced by renewable energies, the frequency response control belongs to hydro-power units. Hence, novel methods are required to enhance the frequency response in power systems with low inertia.

Additionally, the current and future power system communication infrastructure is based on PMUs along the NPS [30]. This will enable the application of WAMS for monitoring the operative areas and to transmit the information required to activate ancillary services for hydro-governors that can counteract the low inertia and enhance the frequency response in time.

### 3.2 Primary frequency response modelling

The objective of a turbine governing system, installed in a generating unit, is to produce a desired power which is partly determined by the set value for the produced power and partly by a contribution originating from the frequency control [31]. In this context, the latter is of interest.

Fig. 3 shows a schematic diagram of the system model which combines the electro-mechanical prime governor, the hydro-turbine, the generator and load. The governor details are provided in the expanded schematic.

The model including the governing system, the servo and the turbine $i$ is given by


This is an open access article published by the IET and Tianjin University under the Creative Commons Attribution-NonCommercial-NoDerivs License
(http://creativecommons.org/licenses/by-nc-nd/3.0/)

$$
\begin{cases}
\dot{\omega}_i = \dfrac{1}{M_i}\left(P_i^{\mathrm{m}} - P_i^{\mathrm{e}} - D_i\omega_i\right) \\
\dot{P}_i^{\mathrm{m}} = -2k_i^{\omega}\dot{\rho}_i^{y} + \dfrac{2k_i^{\omega}}{T_i^{\omega}}\rho_i^{y} - \dfrac{2}{T_i^{\omega}}P_i^{\mathrm{m}} \\
\dot{\rho}_i^{y} = \dfrac{1}{T_i^{\mathrm{p}}}\left(k_i^{\mathrm{t}}\rho_i^{y} - \rho_i^{y}\right) \\
\dot{\rho}_i^{y} = k_i^{\mathrm{i}}\rho_i^{\mathrm{c}} - k_i^{\mathrm{i}}R_i^{\mathrm{p}}\rho_i^{y} + k_i^{\mathrm{p}}\dot{\rho}_i^{\mathrm{c}} - k_i^{\mathrm{p}}R_i^{\mathrm{p}}\dot{\rho}_i^{y} + k_i^{\mathrm{d}}\left(\ddot{\rho}_i^{\mathrm{c}} - R_i^{\mathrm{p}}\ddot{\rho}_i^{y}\right) \\
\dot{\rho}_i^{\mathrm{c}} = \dfrac{1}{T_i^{\mathrm{f}}}\left(\omega_{\mathrm{ref}} - R_i^{\mathrm{f}}\omega_i - \rho_i^{\mathrm{c}}\right)
\end{cases}
\tag{4}
$$

where the constants $T_i^{\mathrm{p}}$, $T_i^{\omega}$, $k_i^{\mathrm{i}}$, $k_i^{\mathrm{p}}$, $T_i^{\mathrm{f}}$, $R_i^{\mathrm{p}}$, $k_i^{\mathrm{t}}$, $M_i$, $D_i$ stand for the servo pilot constant, the water time constant, the integral controller constant, the proportional controller constant, the reset time constant, permanent droop, inertia constant, and damping, respectively.

### 3.3 Stability analysis

In order to guarantee that the hydro-governors remain stable under future improvements, it is necessary to guarantee a stability region.

*Theorem 1:* The power system described by (4) is stable for $k_i^{\mathrm{p}} > 0$ and $k_i^{\mathrm{i}} > 0$.

*Proof:* The stability of (4) is determined by the eigenvalues of $A$. The roots of the characteristic polynomial of $A$ is given by

$$
\begin{gathered}
\det\left(s\mathbf{I} - A_i\right) = 0 \\
\sum_{j=0}^{5} a_j s^j = 0
\end{gathered}
\tag{5}
$$

Since the hydro-governor model used is linear (5), the Routh–Hurwitz stability criterion accomplishes the stability proof (see Section 8). □

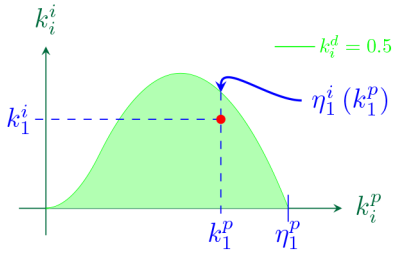


**Fig. 4** *Stability region $\Omega^s$ for the PI governor based*

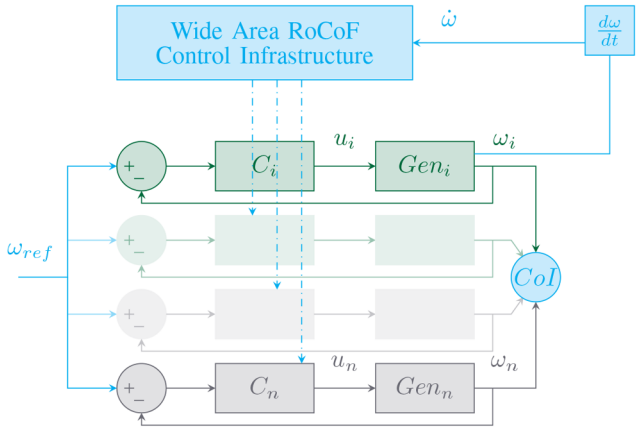


**Fig. 5** *Wide-area control architecture*

Fig. 4 shows a plot of $k_i^{\mathrm{i}}$ versus $k_i^{\mathrm{p}}$ and displays the stability region for the PI governor based. $\eta^{\mathrm{i}}$ stands for a vector of $k_1^{\mathrm{i}}$ and $k_1^{\mathrm{p}}$ parameters that are inside of the stability region $\Omega^{\mathrm{s}}$.

## 4 WARS-based frequency control

In this section a wide area measurement system (WAMS) architecture to counteract the reduction of inertia in power systems by using WARS measurement functions. Additionally, the impact of the communication delay on the stability margins of the system is shown. These constitute the main contributions of this paper.

### 4.1 Wide-area RoCoF sharing

WAMS are used to transmit information and accurate measurements from remote geographical locations throughout the involved power systems. Fig. 5 represents the concept of the proposed method based on WAMS. Each aggregated power system area is measured by a PMU network sparsed in the system, which are connected to the main phasor data concentrator (PDC) via communication channels (shown in dashed lines in Fig. 5) enabling to obtain the CoI measurement by collecting several frequency measurements. Moreover, information from the RoCoF signal is collected and exchanged with the required local controllers (typically <0.2 Hz/s within large power networks) [32].

By exploiting the inertia reduction in one area $i$, caused by the large increasing renewable energy integration, and assuming a communication channel between the other areas in the power network, the RoCoF signal is transmitted. Since an inertia reduction implies a steeper declination in the RoCoF and faster reaction than the local frequency in other regions, sharing this measurement with other regions can improve the global frequency response in the case of undesired disturbances. As can be seen in Fig. 5, an area is being measured and its respective RoCoF is then distributed to the other areas ($\mathrm{Gen}_i$ to $\mathrm{Gen}_n$) and their controllers ($C_i$ to $C_n$); the sum of these results in the CoI frequency. Note that Fig. 5 shows only one area being measured for simplicity. However, all of the areas can be measured and the individual RoCoFs can be distributed to the rest of the areas.

In this application, initially a single CoI per area is assumed, which is represented by an aggregated machine and its dynamic controller. Additionally, in order to observe the effect of the RoCoF sharing on the CoI, the frequency measurements of each aggregated area are clustered and the overall frequency of the systems can be observed as a global CoI. RoCoF area measurements are also derived and shared to the other areas by communication channels.

*4.1.1 RoCoF sharing functions:* Two functions for WAMS RoCoF measurements are proposed as follows:

$$
\mathrm{RoCoF}_{\mathrm{avg}} = \mathrm{avg}(\mathrm{RoCoF}_s, \mathrm{RoCoF}_i) \tag{6}
$$

$$
\mathrm{RoCoF}_{\mathrm{max}} = \max(|\mathrm{RoCoF}_s|, |\mathrm{RoCoF}_i|) \tag{7}
$$

Both functions (6) and (7) take the shared RoCoF measurement (from the RoCoFs networked areas) and combine it with the local $i$ measurement sensed in the respective hydro-governor. Function (6) is obtained by the average of both measurements. On the other hand, function (7) obtains the maximum steepness between those two measurements. By taking the swing equation in (1), both functions are briefly analysed in CoI frame as follows:

$$
\begin{aligned}
2\Sigma H_i \frac{\mathrm{d}(\Sigma_i H_i\omega_i/\Sigma_i H_i)}{\mathrm{d}t} &= \Sigma\Delta P_i \\
2H_{\mathrm{CoI}}\frac{\mathrm{d}\omega_{\mathrm{CoI}}}{\mathrm{d}t} &= \Sigma\Delta P_i
\end{aligned}
\tag{8}
$$

As an example, by applying the CoI frame to a system of two masses with inertias $H_1$ and $H_2$, the following expression is obtained:


This is an open access article published by the IET and Tianjin University under the Creative Commons Attribution-NonCommercial-NoDerivs License
(http://creativecommons.org/licenses/by-nc-nd/3.0/)

$$
\begin{aligned}
2H_{\mathrm{CoI}_T}\frac{\mathrm{d}\omega_{\mathrm{CoI}_T}}{\mathrm{d}t} &= 2H_1\frac{\mathrm{d}\omega_1}{\mathrm{d}t} + 2H_2\frac{\mathrm{d}\omega_2}{\mathrm{d}t} \\
&= 2(H_1+H_2)\left(\frac{H_1}{H_1+H_2}\frac{\mathrm{d}\omega_1}{\mathrm{d}t} + \frac{H_2}{H_1+H_2}\frac{\mathrm{d}\omega_2}{\mathrm{d}t}\right) \\
&= 2(H_1+H_2)\frac{\mathrm{d}((H_1\omega_1+H_2\omega_2)/(H_1+H_2))}{\mathrm{d}t} \\
&= 2\frac{\mathrm{d}(H_1\omega_1+H_2\omega_2)}{\mathrm{d}t}
\end{aligned} \tag{9}
$$

The result in (9) coincides with the CoI definition. By including the proposed average shared function in one of the areas, the new CoI is the following:

$$
2H_{\mathrm{CoI}_{\mathrm{avg}}}\frac{\mathrm{d}\omega_{\mathrm{CoI}_{T\mathrm{avg}}}}{\mathrm{d}t} = 2H_1\frac{\mathrm{d}((H_1\omega_1+H_2\omega_2)/(H_1+H_2))}{\mathrm{d}t} + 2H_2\frac{\mathrm{d}\omega_2}{\mathrm{d}t} \tag{10}
$$

Equation (10) shows the dynamic change in the CoI result where one of the areas has the weighted (average) RoCoF obtained indicating the influence of the function in the local RoCoF and CoI. Note that the RoCoF steepness depends on the inertia delivered in the system. However, the inertia estimation is out of the scope of this document.

Regarding the second function, the maximum of the absolute value of the RoCoF reacts to the steepness, therefore automatically selecting the RoCoF with the higher slope or, in other words, transporting the RoCoF of the area with less inertia. The new CoI changes as follows:

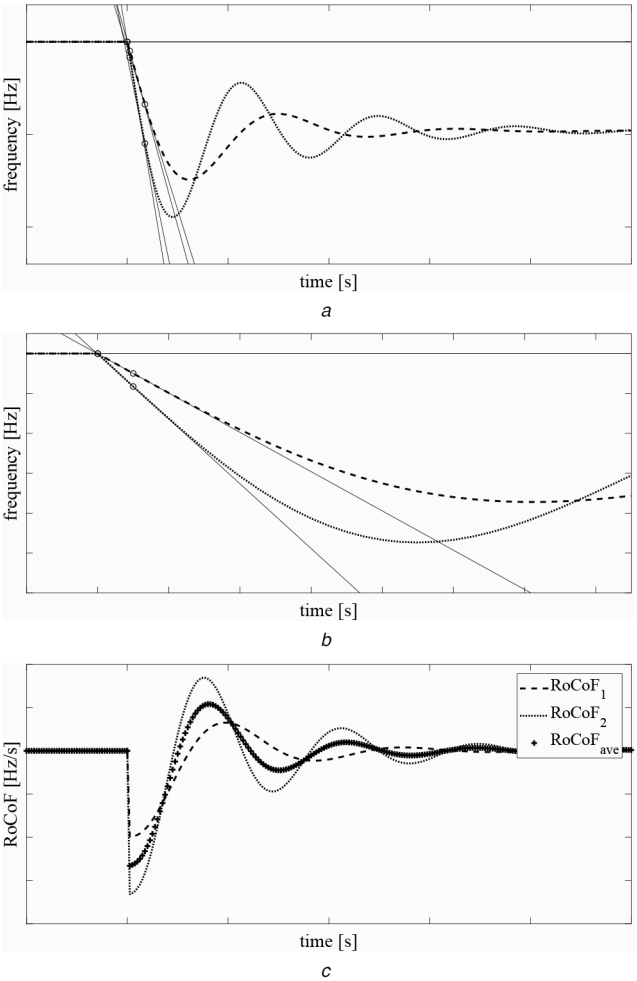


**Fig. 6** *Frequency and RoCoF functions*
***(a)*** Frequency response of two different areas, ***(b)*** Ramp tangent lines, ***(c)*** RoCoF associated

$$
\begin{aligned}
2H_{\mathrm{CoI}_{\max}}\frac{\mathrm{d}\omega_{\mathrm{CoI}_{T\max}}}{\mathrm{d}t} &= 2H_1\frac{\mathrm{d}\omega_2}{\mathrm{d}t} + 2H_2\frac{\mathrm{d}\omega_2}{\mathrm{d}t} \\
&= 2\frac{\mathrm{d}(H_1\omega_2+H_2\omega_2)}{\mathrm{d}t} \\
&= 2\frac{\mathrm{d}(\omega_2(H_1+H_2))}{\mathrm{d}t}
\end{aligned} \tag{11}
$$

Note that (11) compared to the common CoI (9) has changed, and since the RoCoF in the second area is steeper, the dynamic reaction provoked is faster than the average function.

### *4.2 Function signals*

Fig. 6*a* shows the frequency response of two hypothetical areas 1 and 2 after a load increasing. Both frequencies drop instantaneously, however since each sub-system has different inertia constants $H_1$ and $H_2$, the RoCoF responses are also different as shown in Fig. 6*c*. The RoCoF responses have different slope ramps as shown in Fig. 6*b*, where the initial slope lines have been emphasised to show the respective ramp decay at the beginning of the disturbance which are sensed by their respective control systems (governors). When detecting an abrupt frequency drop, the average function between the RoCoF measurements involved will generate a new RoCoF responses as shown in the + line in Fig. 6*c*. However, when the RoCoF decays faster, the frequency slope is decaying faster therefore the maximum RoCoF (RoCoF 1 in this case) function can have a bigger impact on the governors reaction by sharing it. The selection and triggering of any of those functions are autonomously given by the slope thresholds obtained. However, the RoCoF margins depend on the grid code settings per country [33].

### *4.3 Wide area measurements infrastructure*

With the RoCoF sharing functionality installed, each generating unit will be able to respond and support the system during abnormal frequency conditions (FRC-D). The functionality of the RoCoF sharing is straightforward: The generating unit operates normally at a fixed output set by the regional control centre/TSO [34]; if the frequency goes out of range, the generating unit will respond to a frequency change by either increasing/decreasing its output, according to its primary frequency control obligation.

The condition to activate this control from TSO requires the knowledge of the individual RoCoF measurements in the WAMS. Apart from the PMUs and PDC, another key element is required for the RoCoF sharing application: the detection and activation of the RoCoF sharing mode is made in the local controllers. The RoCoF values from the PMUs are used as the process value to the functions that interact with the local controllers. Usually, a programmable logic controller (PLC) with the optimised parameters and the enable RoCoF sharing signals function [35]. The frequency is measured in the closest busbar/substation to the generation point by a PMU and communicated to the common PLC.

The PLC executes the RoCoF block for every 100 ms interval and uses one of the proposed RoCoF functions measured on the previous cycle. If the slope of the frequency deviation between measured and previous frequency sample when calculated for the total time of 1 s is >0.5 Hz then the sharing frequency mode is activated [36]. The common PLC is adjusting (adjustment is done by optimal PID controller gensetwise) by increasing or decreasing the control signals output [37]. The RoCoF values from the PMUs are used as the process value to the functions to modify the controllers. The system will be reset to normal operation mode when the system has been in normal frequency ranges (typically 1 min) or if automatic reset is a disabled system which remains in the emergency mode until it is reset from TSO.

TSO can monitor the maximum and minimum available RoCoF measurements. A PID controller at common physical location (e.g. a PLC) uses any of functions proposed from remote and local feeders and PMU as a process value from TSO. As a default, controller output uses the optimal parameters.


This is an open access article published by the IET and Tianjin University under the Creative Commons Attribution-NonCommercial-NoDerivs License
(http://creativecommons.org/licenses/by-nc-nd/3.0/)

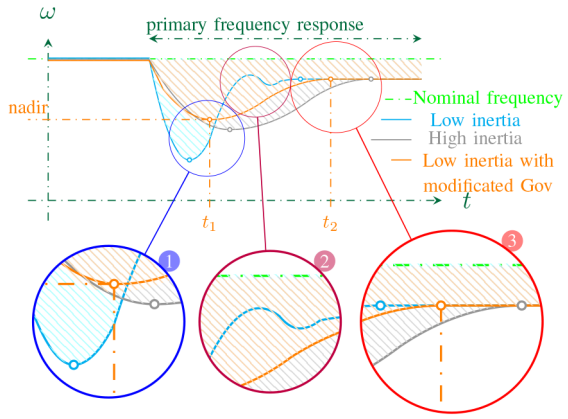


**Fig. 7** *Power system frequency response: Optimisation regions*

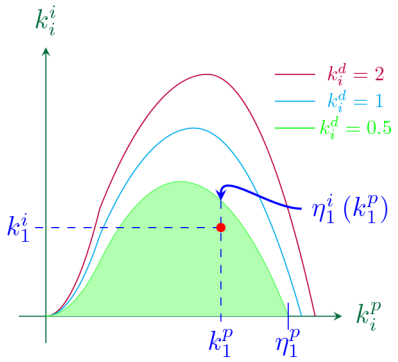


**Fig. 8** *Stability region $\Omega^s$ for a governor PID based: $k_i^d$ variation*

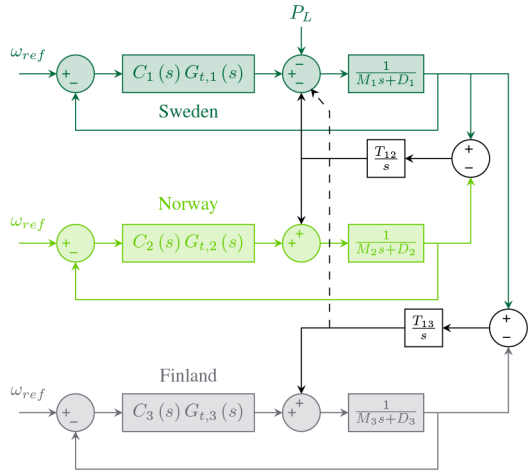


**Fig. 9** *Three mass areas: block diagram*

### 4.4 RoCoF sharing including communication delay

Since the RoCoF sharing application relies on the communication between different operative areas, the delays in the respective communication channels need to be evaluated and measured. A significant delay, of e.g. between 1.0 and 1.6 s, the RoCoF shared area and the receiver area would affect the performance of the expected response and impact on the frequency response individually and the CoI. Timely preventive actions require the a priori knowledge of the delay boundaries that the proposed method and the system can afford. Therefore, a proof of the delay stability margin is calculated and given in Section 10.

## 5 Simulated annealing algorithm application

SAA is a stochastic global optimisation algorithm, which is able to jump out from local minimum to achieve the global minimum [38]. In specific, SAA could be divided into six major components including

i. cost function,
ii. initial condition,
iii. move generation,
iv. probability function,
v. cooling schedule,
vi. stopping condition.

Given a cost function, an initial solution (condition) is generated. Then, in each step, the move generation function will control the perturbation around the current solution. The probability function that is affected by the temperature identifies the acceptance of a new status. Next, the temperature is cooled down to archive a more contingent acceptance criterion for the same probability function; therefore, a worse state is harder to be accepted in the future. Finally, during the SAA procedures, the cost function value eventually converges, and the search is terminated if the stopping condition is satisfied. In this paper, the SAA is used to find the optimal values of the tunable $k^{\mathrm{i}}, k^{\mathrm{p}}, k^{\mathrm{d}}$ to minimise the settling time $t_{\mathrm{s}}$ and the instantaneous frequency deviation (IFD). The corresponding pseudo-algorithm of the applied SAA is presented in Section 9.

### 5.1 Optimisation problem

The formulation of optimisation problem is described as follows:

$$\begin{aligned} &\text{Given } \Omega^{\mathrm{s}} \\ &\text{Min } t_{\mathrm{s}}, \text{nadir}, \\ &\text{s.t.} \quad k^{\mathrm{p}}, k^{\mathrm{i}}, k^{\mathrm{d}} \in \text{stability region} \end{aligned} \tag{12}$$

where $\Omega^{\mathrm{s}}$ is the stability region of each system.

## 6 Study cases

### 6.1 Optimal PID hydro-governor benchmark

The optimisation process aims to obtain optimal parameters that enhance the primary control response such that the time response is minimal and the oscillations are suppressed. These objectives are conflicting, i.e. the more reaction is released to counteract the fall of frequency, the more severe will be the post-support disturbance.

Fig. 7 shows the frequency response versus time for three cases with low inertia, high inertia and low inertia with modified governor. The figure also shows the three time zones where the objective function is operating. Zone 1 focuses on minimising the IFD, Zone 2 looks for avoiding undesired oscillations along the stabilisation. Finally, Zone 3 aims to obtain the minimum settling time such that a faster reaction will be provided.

Having reached the optimal gain parameters in each area, the values should remain inside the stability region in order to guarantee the stability of the system. From the theorem, a theoretical region is shown in Fig. 4. Plane $k_i^{\mathrm{p}}$ versus $k_i^{\mathrm{i}}$ encloses a region where both parameters map a stability point. With the addition of the optimal derivative control parameter, a shift in the region is affected. Therefore, a careful balance of the parameters is considered in the optimal parameters obtained. Fig. 8 shows the representation of this shift on the stability planes by adding the derivative part; the characteristics with three different values of the derivative part $k_i^{\mathrm{d}} = 0.5$, 1 and 2 are shown.

### 6.2 Three mass areas

In order to test the proposed methodology, a test system was created following the parameters in [21]. It represents a Nordic equivalent for frequency studies formed by three-mass areas, as depicted in Fig. 9 and conceptually depicted in Fig. 10 where $\mathrm{Gen_n}$ is the Norway (Norwegian) system, $\mathrm{Gen_s}$ the Sweden (Swedish) system and $\mathrm{Gen_f}$ the Finland (Finnish) system.

The parameters of each area, including the default governor settings before tuning ($k_{\mathrm{p}}$, $k_{\mathrm{i}}$, $k_{\mathrm{d}}$), and the power production in the system are shown in Tables 1 and 2, respectively. Additionally, the


This is an open access article published by the IET and Tianjin University under the Creative Commons Attribution-NonCommercial-NoDerivs License
(http://creativecommons.org/licenses/by-nc-nd/3.0/)

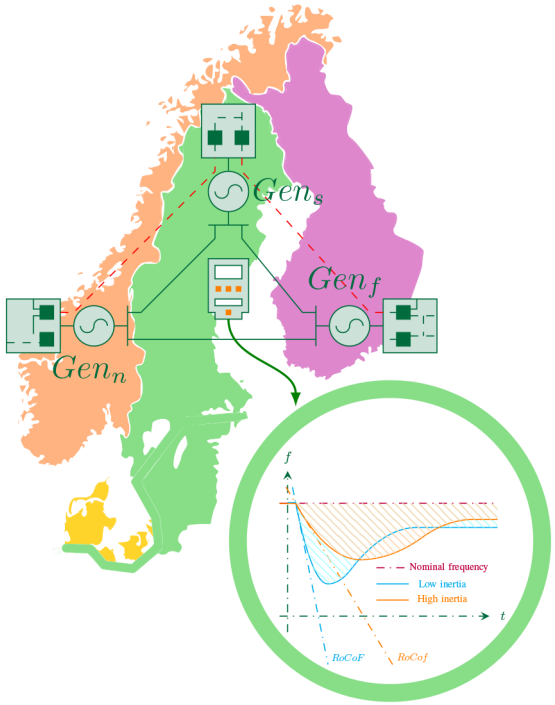


**Fig. 10** *WARS representation*

**Table 1** Hydro-governor parameters

| Parameter | Aggregated model | Sweden | Finland | Norway |
|---|---|---|---|---|
| $k_p$ | 1.6 | 0.25 | 0.08 | 1.27 |
| $k_i$ | 0.175 | 0.0417 | 0.0133 | 0.141 |
| $e_p$ | 0.133 | 0.236 | 1.25 | 0.236 |
| $T_y$ | 0.2 | 0.2 | 0.2 | 0.2 |
| $T_\omega$ | 1.01 | 1.4 | 1.4 | 0.7 |
| $M$ | 9.68 | 4.65 | 1.93 | 3.25 |
| $D$ | 0.517 | 0.246 | 0.087 | 0.184 |

**Table 2** Power production per country

| Production | Sweden | Norway | Finland |
|---|---|---|---|
| MW | 11,620 | 17,825 | 2028 |
| $W_{kin}$ | 112,605 | 81,177 | 48,187 |

**Table 3** Obtained controller parameters by SAA

| Plant | $k_i^p$ | $k_i^i$ | $k_i^d$ |
|---|---|---|---|
| Sweden | 0.56 | 0.07 | 1.85 |
| Norway | 0.8 | 0.05 | 2.34 |
| Finland | 0.07 | 0.02 | 1.05 |

**Table 4** Performance metrics comparison

| | Nadir time | Settling time | $\Delta t$ |
|---|---|---|---|
| base | 12.85 | 46.83 | 33.98 |
| avg | 12.89 | 38.90 | 26.01 |
| max | 13.03 | 34.62 | 21.59 |

1-area aggregated model that represents the entire frequency model system is shown. Note that the default parameters do not contain the derivative controller constant.

As a benchmark, the optimal parameters derived using SAA [39] have been used to evaluate the WARS method. The optimal parameters for the controllers obtained from the SAA are given in Table 3.

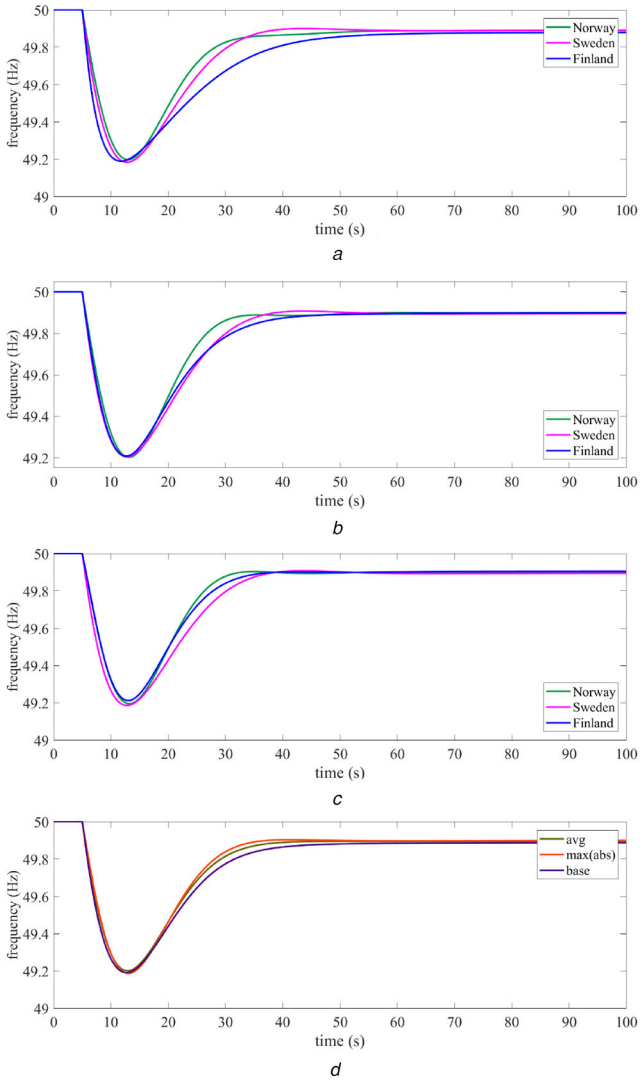


**Fig. 11** *Three areas frequency response with RoCoF sharing*
***(a)*** Frequency response: SAA optimal case, ***(b)*** Sharing RoCoF measurement: average function, ***(c)*** Sharing RoCoF measurement: max function, ***(d)*** Frequency response: CoI

*6.2.1 Frequency response:* By applying the SAA, the optimal governor parameters are found to be based on the criteria established in the benchmark. Fig. 11 shows the time-response comparison between the parameters obtained by the SSA and the methods proposed in each area of the system. Additionally, the CoI response is also given. As can be seen in Figs. 11*b* and *c*, both responses in Norway and Finland reacted faster compared to the optimal case in Fig. 11*a*. The optimal response in Sweden remained the same since it is the one with reduced inertia and sharing its RoCoF measurement through the functions to the other operative areas. By sharing the RoCoF, the frequency response is drastically improved, reducing the overshoot and settling time. Additionally, the CoI response of the two methods proposed in Fig. 11*d* is shown. Optimal response has been improved significantly by the RoCoF sharing in the other two areas since two of them have been improved individually.

Table 4 shows the performance metrics comparison between the SAA optimal parameters and the application of both functions (average and maximum) following the RoCoF measurements. The optimal SAA application has clearly improved the response of the default system. However, with the application of the proposed method functions the relative settling time and $\Delta t$ have been reduced in the overall system response.

*6.2.2 Frequency response with the delay effect:* Fig. 12 shows the variation of the communication delay $\tau$ versus derivative controller gain $k_d$ in Norway and Finland systems. A larger value in the derivative controller gain is less sensitive to the communication


This is an open access article published by the IET and Tianjin University under the Creative Commons Attribution-NonCommercial-NoDerivs License
(http://creativecommons.org/licenses/by-nc-nd/3.0/)

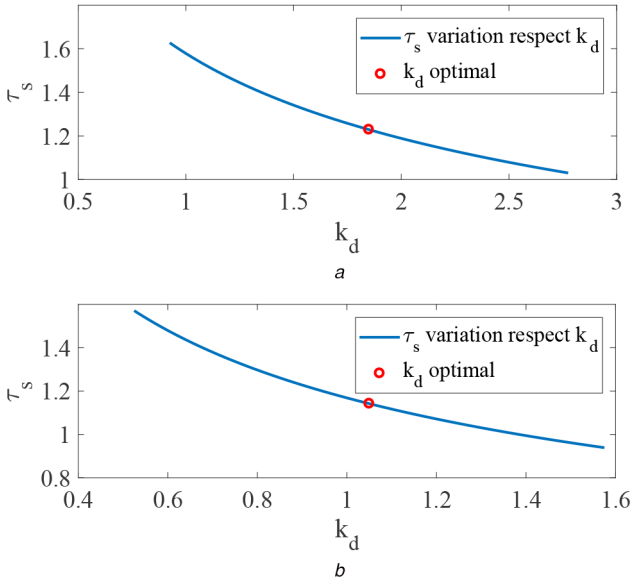


**Fig. 12** *Stability delay regions of the RoCoF shared areas*
***(a)*** Communication delay: RoCoF sharing to Norway, ***(b)*** Communication delay: RoCoF sharing to Finland

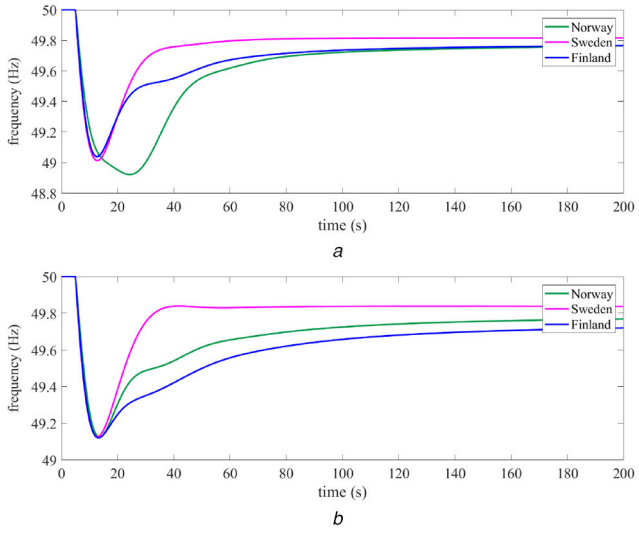


**Fig. 13** *Delay impact on the proposed RoCoF sharing functions*
***(a)*** Delay impact: average function, ***(b)*** Delay impact: max function

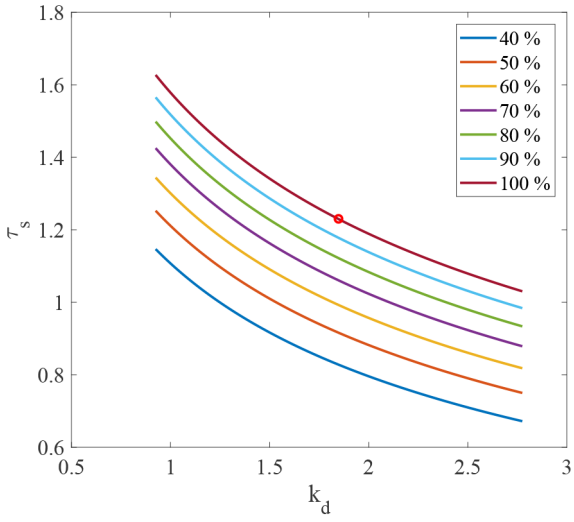


**Fig. 14** *Communication delay and inertia variation in percentage: RoCoF sharing to Norway*

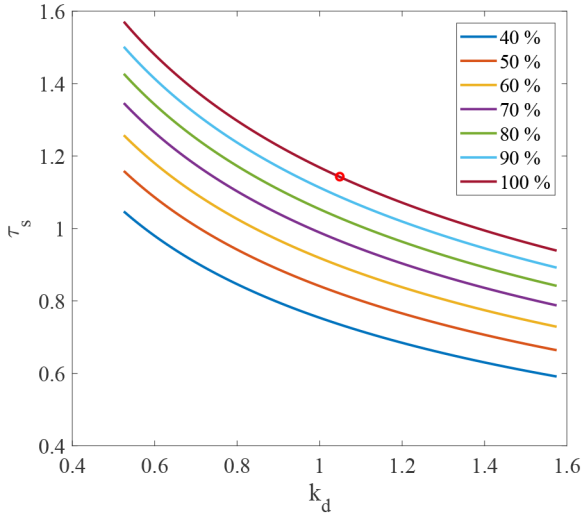


**Fig. 15** *Communication delay and inertia variation in percentage: RoCoF sharing to Finland*

delay in the control signal since its reaction has a larger reaction in a time frame. However, it is clear that an interruption of the signal or a consistent delay will bring the system to an unstable region. Even though the operative areas where the RoCoF measurements have been shared have a similar delay stability region, it is observed that Finland has a larger critical influence in the derivative controller (Fig. 12*b*).

Having found the maximum possible delay in the shared RoCoF signals in the respective operative areas, the impact of such a delay is shown in Fig. 13. Both average and maximum functions and CoI frequency response are clearly affected by the communication delay compromising not only the performance metrics, but the individual responses also. Since in the scenario proposed, Norway has bigger inertia constant, it is less affected, contrary to Finland, whose response becomes oscillatory or out of range of an adequate response. Additionally, the optimal response obtained is also affected.

*6.2.3 RoCoF sharing and delay impact on the inertia:* Additionally, the variation of the inertia $M_i$ parameter of the Norwegian and Finnish areas is shown in Figs. 14 and 15, respectively. In general, as reducing the inertia, the system tolerates a smaller delay within the control action stability region, implying that the control action accepts a lower delay in the information propagation.

## 7 Conclusions

The integration of large amounts of non-synchronous generation in inter-connected power systems is a concern as it leads to a reduction in the net inertia of the overall system. The degradation in the inertia alters the frequency response and provokes different RoCoF slopes in the interconnected systems.

In this paper, an approach to counter-measure the reduction of inertia in power systems is proposed: a novel WAMS based on RoCoF sharing (WARS) to enhance the primary frequency response. Additionally, two functions for the RoCoF sharing method are proposed and compared. The method improves the individual frequency area's response and the CoI response. Moreover, it is analysed the impact of the inertia variation and the delay on the RoCoF sharing showing the regions of stability where the method can be operated.

Further studies require the merge of the so-called synthetic inertia with the share RoCoF and the application to larger power systems; additionally, a study of robust control techniques in delayed dynamical systems.


This is an open access article published by the IET and Tianjin University under the Creative Commons Attribution-NonCommercial-NoDerivs License
(http://creativecommons.org/licenses/by-nc-nd/3.0/)

## 8 Routh–Hurwitz stability proof

From $G(s)$ the terms of the characteristic polynomial are obtained and Routh–Hurwitz's criterion is applied to establish the stability boundaries. Let $a_i$ be the characteristic polynomial coefficients and let $b_i$, $c_i$, $d_i$ and $e_i$ be the Routh–Hurwitz's coefficients. Then, the set $\Omega_s$ is defined by the following constraints problem:

$$\Omega^{s}=\forall\left(k_i^{p},k_i^{i}\right):\begin{cases}\max & u:k_i^{p}+k_i^{i}\\ \text{s.t.} & g_1:a_5>0\\ & g_2:a_4\left(k_i^{p}\right)>0\\ & g_3:a_3\left(k_i^{p},k_i^{i}\right)>0\\ & g_4:a_2\left(k_i^{p},k_i^{i}\right)>0\\ & g_5:a_1\left(k_i^{p},k_i^{i}\right)>0\\ & g_6:a_0\left(k_i^{i}\right)>0\\ & g_7:b_1\left(k_i^{p},k_i^{i}\right)>0\\ & g_8:c_1\left(k_i^{p},k_i^{i}\right)>0\\ & g_9:d_0\left(k_i^{p},k_i^{i}\right)>0\\ & g_{10}:e_0\left(k_i^{i}\right)>0\\ & g_{11}:k_i^{p}>0\\ & g_{12}:k_i^{i}>0\end{cases}\tag{13}$$

## 9 Used SAA pseudo code

See Fig. 16.

## 10 Delay stability proof

A delay time $\tau$ has been introduced though the between the shared RoCoF and the local RoCoF measurement reflected in the derivative control action refereed to Fig. 3. This addition implies modification in the systems neutral delay differential equation (NDDE) system representation [40]. The state variable $\rho_i^{y}$ is defined as

$$\dot{\rho}_i^{y}=k_i^{i}\rho_i^{c}-k_i^{i}R_i^{p}\rho_i^{y}+k_i^{p}\dot{\rho}_i^{c}-k_i^{p}R_i^{p}\dot{\rho}_i^{y}+k_i^{d}s\left(\dot{\hat{\rho}}_i^{c}-R_i^{p}\dot{\hat{\rho}}_i^{y}\right)\tag{14}$$

The general structure of a linear system is described by NDDEs with $\tau\geq 0$ is

$$\dot{\boldsymbol{x}}_i(t)-\sum_{k=1}^{q}\boldsymbol{B}_{i_k}\dot{\boldsymbol{x}}_i(t-k\tau)=A_{i_0}\boldsymbol{x}_i(t)+\sum_{k=1}^{q}\boldsymbol{A}_{i_k}\boldsymbol{x}(t-k\tau),\quad \tau\geq 0\tag{15}$$

1: **Select** an initial state $i\in S$;
2: **Select** an initial temperature $T_i>0$;
3: **Set** temperature change counter $t=0$;
4: *Repeat*
5: **Set** repetition counter $n=0$;
*Repeat* **Generate** state $j$, a neighbor of $i$; **Calculate** $\delta=f(j)-f(i)$; *If* $\delta<0$ then $i:=j$ *else if* $random(0,1)<exp(-8/T)$ then $i:=j$;
$n:=n+l$;
*until* $n=N(t)$;
6: $t:=t+l$;
7: $T:=T(t)$;
8: *until* stopping criterion true.
9: **return** $T$

**Fig. 16** *Algorithm 1: SAA pseudo code*

Having $q=1$ and $\hat{x}_i=x_i(t-\tau)$, the NDDE structure in the state space is given by

$$\dot{\boldsymbol{x}}_i(t)-\boldsymbol{B}_{i_1}\dot{\hat{\boldsymbol{x}}}_i=A_{i_0}\boldsymbol{x}_i(t)+\boldsymbol{A}_{i_1}\hat{\boldsymbol{x}}_i,\quad \tau\geq 0\tag{16}$$

$$\boldsymbol{A}_{i_1}=\begin{bmatrix}0 & 0 & 0 & 0 & 0\\ 0 & 0 & 0 & 0 & 0\\ 0 & 0 & 0 & 0 & 0\\ \dfrac{k_i^{d}R_i^{f}}{T_i^{f}}\left(\dfrac{1}{T_i^{f}}+\dfrac{D_i}{M_i}\right) & -\dfrac{k_i^{d}R_i^{f}}{T_i^{f}M_i} & -\dfrac{k_i^{d}R_i^{p}}{T_i^{f^2}} & \dfrac{k_i^{d}R_i^{p}k_i^{t}}{T_i^{p^2}} & \dfrac{k_i^{d}}{T_i^{f^2}}\\ 0 & 0 & 0 & 0 & 0\end{bmatrix}\tag{17}$$

$$\boldsymbol{B}_{i_1}=\begin{bmatrix}0 & 0 & 0 & 0 & 0\\ 0 & 0 & 0 & 0 & 0\\ 0 & 0 & 0 & 0 & 0\\ 0 & 0 & 0 & -\dfrac{k_i^{d}R_i^{p}k_i^{t}}{T_i^{p}} & 0\\ 0 & 0 & 0 & 0 & 0\end{bmatrix}\tag{18}$$

The characteristic polynomial of system (16) is then

$$p_3(s,\mathrm{e}^{-\tau s})=\det\left[s\left(\boldsymbol{I}-\boldsymbol{B}_{i_1}\mathrm{e}^{-\tau s}\right)-A_{i_0}-A_{i_1}\mathrm{e}^{-\tau s}\right],\quad \tau\geq 0\tag{19}$$

The neutral part of the system is required to be stable:

$$\boldsymbol{x}-\boldsymbol{B}_{i_1}\hat{\boldsymbol{x}}=0\tag{20}$$

Equation (20) is stable for $\tau\geq 0$ if and only if $\rho(\boldsymbol{N}_s)<1$. Now, $\boldsymbol{N}_s=\boldsymbol{B}_{i_1}$ and having the delay $\tau$ involved, then

$$\rho(\boldsymbol{N}_s)=\max\{|\lambda_1|,\ldots,|\lambda_5|\}=\frac{k_i^{d}R_i^{p}k_i^{t}}{T_i^{p}}<1\tag{21}$$

From (21) the maximum tolerance limit for $k_i^{d}$ is extracted as

$$k_i^{d}<\frac{T_i^{p}}{R_i^{p}k_i^{t}}\tag{22}$$

From (21), the delay margin is given by

$$\tau_i^{s}=\inf\left\{\tau:p\left(s,\mathrm{e}^{-\tau_i s}\right)=0,\ \text{for } a\ s\in\bar{\mathbb{C}}_{>0}\right\}\tag{23}$$

With $n=5$, $q=1$ and $B_{i_0}=0$ is having $k=0,1,\ldots,2$:

$$\boldsymbol{H}_k=\sum_{j=\max\{0,k-1\}}^{\min\{k,1\}}\left[\boldsymbol{A}_{i_{k-j}}\otimes\boldsymbol{B}_{i_{1-j}}^{\top}+\boldsymbol{B}_{i_{k-j}}\otimes\boldsymbol{A}_{i_{1-j}}^{\top}\right]\tag{24}$$

$$\boldsymbol{Q}_k=\begin{cases}\boldsymbol{I}\otimes\boldsymbol{A}_{i_{1-k}}^{\top}-\boldsymbol{H}_k,\ k=0\\ \boldsymbol{A}_{i_0}\oplus\boldsymbol{A}_{i_0}^{\top}-\boldsymbol{H}_k,\ k=1\\ \boldsymbol{A}_{i_{k-1}}\otimes\boldsymbol{I}-\boldsymbol{H}_k,\ k=2\end{cases}\tag{25}$$

Matrices $\boldsymbol{U}$ and $\boldsymbol{V}$, as well as $\boldsymbol{\Xi}(z)$, are given by

$$\boldsymbol{U}=\begin{bmatrix}\boldsymbol{I} & \boldsymbol{0}\\ \boldsymbol{0} & \boldsymbol{Q}_2\end{bmatrix}\tag{26}$$

$$\boldsymbol{V}=\begin{bmatrix}\boldsymbol{0} & \boldsymbol{\mathrm{I}}\\ -\boldsymbol{Q}_0 & -\boldsymbol{Q}_1\end{bmatrix}\tag{27}$$

$$\boldsymbol{\Xi}(z)=\left(\boldsymbol{I}-\boldsymbol{B}_{i_1}z\right)^{-1}\left(\boldsymbol{A}_{i_0}+\boldsymbol{A}_{i_1}z\right)\tag{28}$$


This is an open access article published by the IET and Tianjin University under the Creative Commons Attribution-NonCommercial-NoDerivs License
(http://creativecommons.org/licenses/by-nc-nd/3.0/)

Note $\boldsymbol{U}$ and $\boldsymbol{V}$ are of dimensions $50 \times 50$. The stability margin with the delay $\tau_i^{\mathrm{s}}$ is defined with the following steps:

- if $\sigma(\boldsymbol{V}, \boldsymbol{U}) \cap \partial\mathbb{D} = \varnothing$, then $\tau_i^{\mathrm{s}} \to \infty$;
- if not, if $\sigma(\boldsymbol{\Xi}(z_k)) = \{0\}$, $\forall z_k \in \sigma(\boldsymbol{V}, \boldsymbol{U}) \cap \partial\mathbb{D}$, then $\tau_i^{\mathrm{s}} \to \infty$;
- if not, with $m \leq 25$, then

$$\sigma(\boldsymbol{V}, \boldsymbol{U}) \cap \partial\mathbb{D} = \left\{ \mathrm{e}^{\mathrm{j}\alpha_k} : \alpha_k \in [0, 2\pi], k = 1, \ldots, m \right\} \quad (29)$$

  if $\sigma\left(\boldsymbol{\Xi}\left(\mathrm{e}^{-\mathrm{j}\alpha_k}\right)\right) \cap \partial\mathbb{C}_{>0} = \varnothing$, $\forall k = 1, \ldots, m$, then $\tau_i^{\mathrm{s}} \to \infty$;
- else, with $\omega_k^{(i)} \in \mathbb{R}_{>0}$, $\omega_k^{(i)} \neq 0$, and $\mathrm{j}\omega_k^{(i)} \in \sigma\left(\boldsymbol{\Xi}\left(\mathrm{e}^{-\mathrm{j}\alpha_k}\right)\right) \cap \partial\mathbb{C}_{>0}$, $\forall i = 1, \ldots, l$; $l \leq m$, then

$$\tau_i^{\mathrm{s}} = \min_k \ \min_i \frac{\alpha_k}{\omega_k^{(i)}} \quad (30)$$

## 11 References


[1] Chamorro, H.R., Ordonez, C.A., Peng, J.C., *et al.*: 'Nonsynchronous generation impact on power systems coherency', *IET Gener. Transm. Distrib.*, 2016, **10**, (10), pp. 2443–2453

[2] Lin, Z., Wen, F., Ding, Y., *et al.*: 'Wide-area coherency identification of generators in interconnected power systems with renewables', *IET Gener. Transm. Distrib.*, 2017, **11**, (18), pp. 4444–4455

[3] Zhang, G., Cheng, Y., Lu, N., *et al.*: 'Research of hydro-turbine governor supplementary control strategy for islanding ac grid at sending terminal of HVDC system', *IEEE Trans. Energy Convers.*, 2016, **31**, pp. 1229–1238

[4] Chamorro, H.R., Ordonez, C.A., Peng, J.C.-H., *et al.*: 'Coherency estimation in power systems: a koopman operator approach', in Blondin, M.J., Pardalos, P.M., Sanchis Sez, J. (eds.): '*Computational intelligence and optimization methods for control engineering*', Springer optimization and its applications (Springer International Publishing), pp. 201–225

[5] Ackermann, T., Prevost, T., Vittal, V., *et al.*: 'Paving the way: a future without inertia is closer than you think', *IEEE Power Energy Mag.*, 2017, **15**, pp. 61–69

[6] Miller, N.W.: 'Keeping it together: transient stability in a world of wind and solar generation', *IEEE Power Energy Mag.*, 2015, **13**, pp. 31–39

[7] Krpan, M., Kuzle, I.: 'Introducing low-order system frequency response modelling of a future power system with high penetration of wind power plants with frequency support capabilities', *IET Renew. Power Gener.*, 2018, **12**, (13), pp. 1453–1461

[8] Singh, M.K., Naresh, R., Gupta, D.K.: 'Optimal tuning of temporary droop governor of hydro power plant using genetic algorithm'. 2013 Int. Conf. on Energy Efficient Technologies for Sustainability, Nagercoil, India, April 2013, pp. 1132–1137

[9] Abdolmaleki, M., Ranjbar, A.M., Ansarimehr, P., *et al.*: 'Optimal tuning of temporary droop structure governor in the hydro power plant'. 2008 IEEE 2nd Int. Power and Energy Conf., Johor Bahru, Malaysia, December 2008, pp. 100–105

[10] Shayeghi, H., Molaee, A., Valipour, K., *et al.*: 'Multi-source power system fopid based load frequency control with high-penetration of distributed generations'. 2016 21st Conf. on Electrical Power Distribution Networks Conf. (EPDC), Karaj, Iran, April 2016, pp. 131–136

[11] Sun, X., Fang, H.: 'Speed governor pid gains optimal tuning of hydraulic turbine generator set with an improved artificial fish swarm algorithm'. 2016 IEEE Int. Conf. on Information and Automation (ICIA), Zhejiang, China, August 2016, pp. 2033–2035

[12] Liu, S., Li, D., Huang, C.e: 'Nonlinear robust control with high gain observer for governor of hydro-turbine generator sets'. Proc. of the 10th World Congress on Intelligent Control and Automation, Beijing, China, July 2012, pp. 2752–2757

[13] Qing, D., Xiangwu, Y.: 'Evaluate the effect of hydro turbine governor decentralized control by transient energy'. 2006 Chinese Control Conf., August 2006, pp. 1655–1659

[14] Yang, F., Lei, H., Sun, Y., *et al.*: 'Control of hydraulic turbine generators using exact feedback linearization'. IEEE ICCA 2010, Xiamen, China, June 2010, pp. 1372–1378

[15] Eker, İ.: 'Governors for hydro-turbine speed control in power generation: a SIMO robust design approach', *Energy Convers. Manage.*, 2004, **45**, pp. 2207–2221

[16] Sami, A., Kadri, M.B., Aziz, N., *et al.*: 'Design simulation of fuzzy PID for hydro power plant'. 2016 Sixth Int. Conf. on Innovative Computing Technology (INTECH), Dublin, Ireland, August 2016, pp. 683–687

[17] Miller, N.W., Delmerico, R.W., Kuruvilla, K., *et al.*: 'Frequency responsive controls for wind plants in grids with wind high penetration'. 2012 IEEE Power and Energy Society General Meeting, San Diego, USA, July 2012, pp. 1–7

[18] Xia, J., Dyko, A., O'Reilly, J.: 'Future stability challenges for the UK network with high wind penetration levels', *IET Gener. Transm. Distrib.*, 2015, **9**, (11), pp. 1160–1167

[19] Wilson, D., Yu, J., Al-Ashwal, N., *et al.*: 'Measuring effective area inertia to determine fast-acting frequency response requirements', *Int. J. Electr. Power Energy Syst.*, 2019, **113**, pp. 1–8

[20] Flores, W.C., Barrionuevo, J., Atlas, E., *et al.*: 'An approach based on remedial action scheme to increase resiliency under failures in the central American power grid'. 2017 IEEE PES Innovative Smart Grid Technologies Conf. – Latin America (ISGT Latin America), Quito, Ecuador, September 2017, pp. 1–6

[21] Saarinen, L., Norrlund, P., Lundin, U., *et al.*: 'Full-scale test and modelling of the frequency control dynamics of the nordic power system'. 2016 IEEE Power and Energy Society General Meeting (PESGM), Boston, USA, July 2016, pp. 1–5

[22] Xi, J., Chamorro, H.R., Persson, J., *et al.*: 'On the influence of the backlash governor settings on the frequency response in power systems'. 2016 IEEE PES Asia-Pacific Power and Energy Engineering Conf. (APPEEC), Xi'an, China, October 2016, pp. 732–737

[23] Chamorro, H.R., Sanchez, A.C., Pantoja, A., *et al.*: 'A network control system for hydro plants to counteract the non-synchronous generation integration', *Int. J. Electr. Power Energy Syst.*, 2019, **105**, pp. 404–419

[24] Gonzalez-Longatt, F., Sanchez, F., Leelaruji, R.: 'Unveiling the character of the frequency in power systems'. 2019 IEEE PES GTD Grand Int. Conf. and Exposition Asia (GTD Asia), Bangkok, Thailand, March 2019, pp. 57–62

[25] Das, K., Litong-Palima, M., Maule, P., *et al.*: 'Adequacy of frequency reserves for high wind power generation', *IET Renew. Power Gener.*, 2017, **11**, (8), pp. 1286–1294

[26] Giovanelli, C., Kilkki, O., Sierla, S., *et al.*: 'Task allocation algorithm for energy resources providing frequency containment reserves', *IEEE Trans. Ind. Inf.*, 2019, **15**, pp. 677–688

[27] Holttinen, H., Ivanova, A., Dominguez, J.L.: 'Wind power in markets for frequency support services'. 2016 13th Int. Conf. on the European Energy Market (EEM), Porto, Portugal, June 2016, pp. 1–5

[28] Pursiheimo, E., Holttinen, H., Koljonen, T.: 'Path toward 100energy future and feasibility of power-to-gas technology in nordic countries', *IET Renew. Power Gener.*, 2017, **11**, (13), pp. 1695–1706

[29] Ostman, K., Hesamzadeh, M.R.: 'Transmission pricing in interconnected systems – a case study of the nordic countries'. 2014 IEEE Int. Energy Conf. (ENERGYCON), Dubrovnik, Croatia, May 2014, pp. 1480–1486

[30] Vanfretti, L., Bengtsson, S., Peric, V.S., *et al.*: 'Spectral estimation of low-frequency oscillations in the nordic grid using ambient synchrophasor data under the presence of forced oscillations'. 2013 IEEE Grenoble Conf., Grenoble, France, June 2013, pp. 1–6

[31] Jin, M.J., Hu, W., Liu, F., *et al.*: 'Nonlinear co-ordinated control of excitation and governor for hydraulic power plants', *IEE Proc. Gener. Transm. Distrib.*, 2005, **152**, pp. 544–548

[32] Roscoe, A.J., Dyko, A., Marshall, B., *et al.*: 'The case for redefinition of frequency and RoCoF to account for ac power system phase steps'. 2017 IEEE Int. Workshop on Applied Measurements for Power Systems (AMPS), Liverpool, UK, September 2017, pp. 1–6

[33] Rate of Change of Frequency (RoCoF) withstand capability – ENTSO-E guidance document for national implementation for network codes on grid connection. 2018

[34] Zhan, S., Xinzhan, L., Yu, H., *et al.*: 'Real-time active power control method of regional power grid considering wind power fluctuations under cps framework'. 2018 Int. Conf. on Power System Technology (POWERCON), November 2018, pp. 2979–2983

[35] Mircescu, D., Astilean, A., Ghiran, O.: 'Complex automation system of a low power hydroplant'. Proc. of 2012 IEEE Int. Conf. on Automation, Quality and Testing, Robotics, Cluj-Napoca, Romania, May 2012, pp. 616–620

[36] Estrada-Estrada, J.H., Ustariz-Farfan, A.J., Cano-Plata, E.A.: 'Application of complexity theory to hydro-turbine maintenance'. 2017 IEEE Workshop on Power Electronics and Power Quality Applications (PEPQA), Bogotá, Colombia, May 2017, pp. 1–6

[37] Skoczowski, S., Domek, S., Pietrusewicz, K., *et al.*: 'A method for improving the robustness of pid control', *IEEE Trans. Ind. Electron.*, 2005, **52**, pp. 1669–1676

[38] Ho, S.L., Yang, S., Wong, H.C., *et al.*: 'A simulated annealing algorithm for multiobjective optimizations of electromagnetic devices', *IEEE Trans. Magn.*, 2003, **39**, pp. 1285–1288

[39] Laarhoven, P.W.: '*Simulated annealing: theory and applications*' (MIT Press, Boston, Mass., U.A., 1987). OCLC: 255505178

[40] Fu, P., Niculescu, S., Chen, J.: 'Stability of linear neutral time-delay systems: exact conditions via matrix pencil solutions', *IEEE Trans. Autom. Control*, 2006, **51**, pp. 1063–1069




This is an open access article published by the IET and Tianjin University under the Creative Commons Attribution-NonCommercial-NoDerivs License
(http://creativecommons.org/licenses/by-nc-nd/3.0/)